Available online at www.sciencedirect.com
SCIENCE DIRECT®
International Journal of Multiphase Flow 30 (2004) 499–520
International Journal of Multiphase Flow
www.elsevier.com/locate/ijmulflow

# Break-up dynamics and drop size distributions created from spiralling liquid jets

D.C.Y. Wong [a], M.J.H. Simmons [a,*], S.P. Decent [b], E.I. Parau [b], A.C. King [b]

[a] Department of Chemical Engineering, The University of Birmingham, Edgbaston, Birmingham B15 2TT, UK
[b] School of Mathematics and Statistics, The University of Birmingham, Edgbaston, Birmingham B15 2TT, UK

Received 20 August 2003; received in revised form 28 March 2004

**Abstract**

The dynamics of the break-up of spiralling jets of Newtonian liquids were visualised. The jets were created from orifices at the bottom of a 0.085-m-diameter can rotating about its vertical axis and imaged using a high-speed camera. The effects of liquid dynamic viscosity (0.001–0.09 Pa s), rotation rate (5–31 rad $s^{-1}$) and orifice size (0.001 and 0.003 m) upon the jet break-up and drop size distributions produced in the Rayleigh regime were investigated. The ranges of dimensionless parameters were $1 < Re < 10^3$, $0.2 < Rb < 4$, $0.5 < We < 25$ and $5 \times 10^{-3} < Oh < 4 \times 10^{-1}$. Four generic break-up modes identified were a strong function of dynamic viscosity and jet exit velocity. A flow pattern map of Ohnesorge number against Weber number enabled prediction of these modes. Increasing the can rotation rate increases jet exit velocity due to centrifugal forces and the trajectory of the jet becomes more curved. The break-up dynamics of the jets were non-linear, although some agreement between measured break-up lengths with the linear stability analysis developed previously was noted at low Reynolds numbers. A non-linear theoretical analysis is required to elucidate the important features.


*Keywords:* Surface tension instability; Prilling; Jet break-up; Drop size distribution; Spiralling jet; High-speed imaging

## 1. Introduction

The creation of drops and sprays from the growth of surface tension instabilities on the surface of liquid jets has been exploited in both industrial applications and scientific research. Many fundamental experimental and theoretical studies on the break-up dynamics of

* Corresponding author. Tel.: +44-121-414-5371; fax: +44-121-414-5324.
*E-mail address:* m.j.simmons@bham.ac.uk (M.J.H. Simmons).

0301-9322/$ - see front matter © 2004 Elsevier Ltd. All rights reserved.
doi:10.1016/j.ijmultiphaseflow.2004.04.002

straight liquid jets have been done over the last century and the work of Savart (1833), Rayleigh (1878) and Weber (1931) is now considered as classical. These are reviewed in detail by Eggers (1997).

However, industrial applications of these phenomena have suffered from the fact that the break-up of the jets usually produces a non-uniform distribution of drop sizes due to non-linearity in the wave growth on the jet's surface. This causes the production of smaller, unwanted satellite droplets which are formed in-between the larger main droplets. For a straight, free falling jet under gravity, the size of the primary drops and jet break-up length are a function of the jet velocity, $U$ (Blaisot and Adeline, 2003). At low jet velocities, primary drops are formed by capillary pinching and aerodynamic forces caused by the influence of the ambient air moving over the jet surface (*wind*) are negligible. This corresponds to the break-up dynamics described by Rayleigh (1878). An increase in jet velocity in this regime causes the break-up length of the jet to increase. The size of the primary drops are generally of the order of the jet diameter. At higher values of $U$, aerodynamic forces and the internal flows within the jet have increased influence (Lin and Lian, 1990; Ohnesorge, 1936); the so-called Taylor or atomisation regime. The primary drops produced in this regime are much smaller.

Bousfield et al. (1986) performed experiments which showed that the relative sizes of the primary and satellite droplets depend strongly on the wave number of the disturbance. Camelot et al. (1999) reported that the mechanism of jet break-up affected the drop size distributions produced. They reported that the mode of instability causing jet break-up changed from *varicose* (axisymmetrical) to *kink* (non-axisymmetrical) with increasing flow rate and liquid physical properties; the latter break-up mechanism produced a much narrower size distribution of main droplets. An increase in the number of satellites produced between two main droplets was also found with increasing flow rate. Blaisot and Adeline (2003) suggested that the formation of kink instabilities are due to the increasing influence of aerodynamic forces, i.e., wind.

More recent experimental studies have been devoted to obtaining methods to reduce the formation of satellites and hence to produce uniformly size droplets (Lindblad and Schneider, 1965; Donnelly and Glaberson, 1965; Goedde and Yuen, 1970) and on obtaining understanding of the non-linear effects of capillary growth (Torpey, 1989; Rutland and Jameson, 1971; Taub, 1976). These studies have led to many workers considering the application of mechanical or sonic disturbances in order to force a particular break-up mode. For example, Chaudhary and Redekopp (1980) successfully applied a sinusoidal disturbance with an added harmonic to suppress the occurrences of satellite droplets. Shield et al. (1987) and Bousfield and Denn (1987) developed the "drop-on-demand" technique, a method which generates individual droplets by pulsing the liquid flow. This technique is limited to a lower droplet production rate than the "continuous" methods of droplet generation where droplets are formed by the growth of surface tension driven instabilities on the surface of a continuous jet.

Theoretical examination of the break-up behaviour of straight jets has developed in parallel to the experimental studies. Linear stability theory can provide qualitative descriptions of break-up phenomena by elucidating the wavelength of the fastest growing wave in the Rayleigh regime. Rayleigh (1878) developed a linear analysis for the growth of axisymmetric temporal disturbances. Keller et al. (1973) considered growth of disturbances in both time and space to allow prediction of the break-up length of straight jets. Non-linear studies, which model the

propagation of finite amplitude disturbances which originate at the orifice, enable the onset of unstable waves over a range of wave numbers and length scales to be predicted. Hilbing and Heister (1996) developed a boundary element method to investigate the non-linear evolution and droplet formation of a straight liquid jet emerging from an orifice, in the absence of gravity, up to the point of pinch-off. Their results showed good agreement with the experiments of Moses (1995).

This work is not directly applicable to more complex jet configurations where the trajectory of the jet is curved, for which there is a comparative paucity of published information. Liquid jets can be curved by the action of gravity, wind drag or if the orifice from which the jet emerges is spinning. Study of curved jets is important since their break-up forms the basis of the industrially important *prilling process* which is used to create products such as fertilizer and magnesium pellets. In this process, urea or magnesium melt flows into a rotating container which has a perforated wall near to its base. Due to centrifugal forces, the melt is flung outwards to the walls and flows through the perforations. On emerging from the perforations, spiralling liquid jets are formed, which break-up into droplets. Prilled fertilizer typically has a size range from 0.001 to 0.0024 m (Meessen and Petersen, 1996). Understanding of the mechanisms of jet break-up in this process is necessary since it is commercially important to be able to produce pellets which are of a closely defined size range. Indeed, the creation of over-fine particles of magnesium may have explosive consequences. Careful control of jet break-up could lead to more uniform particle size distributions, eliminate the creation of fines and hence improve the bulk storage and transportation properties of the product.

Wallwork et al. (2002) developed a linear stability analysis for curved jets. The problem was formulated using the usual continuity equation, the Newtonian Navier–Stokes equations, the kinematic condition on the free surface, normal and tangential stress boundary conditions on the free surface and an arc length condition. To obtain the curvature of the jet, a novel curved variant of cylindrical polar coordinates was introduced. These equations are derived in Wallwork (2002). Following their work, Decent et al. (2002) extended their modelling of free liquid jets by incorporating a gravity term. Use of linear stability theory allowed prediction of the trajectory of the curved jet and the break-up length similar to the work by Middleman (1995) and others developed for straight jets. Nevertheless, they noted that non-linear effects during break-up will become important. In their opinion, a fully non-linear analysis is required to understand the formation of droplets from a spinning liquid jet, an argument addressed in this paper.

This paper presents a parametric study which was done to investigate various aspects of the behaviour of spiralling jets in a break-up regime equivalent to the Rayleigh regime for straight jets, i.e., where the dominant break-up mechanism is by capillary pinch-off and the influences of wind and internal flow within the jet are negligible. The precise jet break-up mechanism, jet exit angle, jet break-up length and the size distributions of the droplets formed were measured over a range of operating parameters and compared with the existing linear stability theory described by Wallwork et al. (2002) and Decent et al. (2002). The parameters varied were the liquid physical properties (density, dynamic viscosity, surface tension), the rotation rate of the spinning can and the size of the orifice from which the jet emerged. The parameter ranges are shown in Table 1.

Table 1
Summary of test conditions

| Parameter | Range |
|---|---|
| Liquid dynamic viscosity, $\eta$ (Pa s) | 0.001–0.081 |
| Liquid density, $\rho$ (kg m$^{-3}$) | 1000–1200 |
| Liquid surface tension, $\sigma$ (N m$^{-1}$) | 0.047–0.072 |
| Orifice radius, $a$ (m) | 0.001 and 0.003 |
| Liquid aspect ratio ($H/D$) | $\frac{2}{3}$–$1\frac{1}{4}$ |
| Can rotation rate, $\Omega$ (rad s$^{-1}$) | 5.2–31.4 (50–300 rpm) |
| Jet exit velocity, $U$ (m s$^{-1}$) | 0.318–0.985 |
| Can radius, $s_o$ (m) | 0.0425 |
| $Rb = \frac{U}{\Omega s_o}$ | 0.2–4.0 |
| $Re = \frac{\rho U a}{\eta}$ | 1–$10^3$ |
| $Fr/Rb = \frac{\Omega s_o}{\sqrt{gH}}$ | 0–2 |
| $We = \frac{\rho U^2 a}{\sigma}$ | 0.5–25 |
| $Oh = \frac{\eta}{\sqrt{\sigma a \rho}}$ | $5\times10^{-3}$–$4\times10^{-1}$ |

## 2. Experimental procedure and apparatus

A schematic diagram of the experimental set-up is shown in Fig. 1. The apparatus used consists of a cylindrical can with a diameter, $D$, of 0.085 m and a height, $H$, of 0.115 m. It contains two diametrically opposed orifices with diameters of 0.001 and 0.003 m, respectively. The can was partially filled to give liquid aspect ratios ($H/D$) ranging from $\frac{2}{3}$ to $1\frac{1}{4}$ and the liquid level was kept constant by supplying fresh solution continuously using a peristaltic pump (Waltson-Marlow 505s).

The trajectory of a jet was captured by means of a high speed digital camera (Photron Fastcam Super 10k), which is capable of recording at up to 10,000 frames per second. The images from the camera were downloaded into a personal computer for analysis. Digital measurements accurate to a tenth of a millimetre were then obtained from the images using Image-Pro Express software (Datacell Ltd., UK). At least 35 frames were examined to ascertain the break-up length. At each

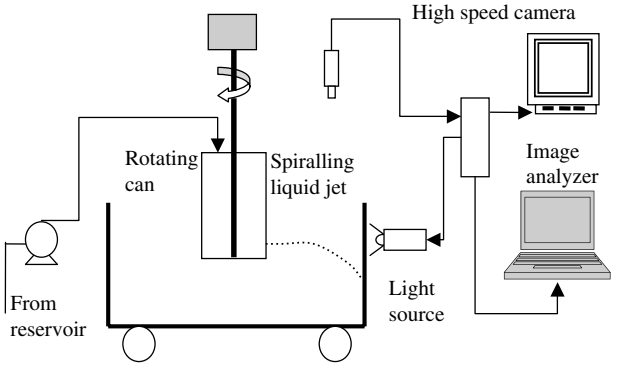


Fig. 1. Spiralling jet experimental set-up.

condition, the reproducibility of experiments was checked by repeating three times. The average exit velocity of the jet leaving the orifice was calculated by dividing the total volume of liquid collected over a period of 1 min by the cross-sectional area of the hole. Liquid physical properties such as density, viscosity and surface tension of the fluid were measured prior to and after the experiments.

The physical properties of the liquid phase were altered by using different fluids. At the conditions present in the industrial process, the density, surface tension and dynamic viscosity of a urea melt are given by Meessen and Petersen (1996) as 1247 $kg\,m^{-3}$, 0.0663 $N\,m^{-1}$ and 0.003 Pa s, respectively. In these experiments, solutions of water and glycerol (0–80% glycerol by volume) were used which gave liquid dynamic viscosities ranging from 0.001 to 0.09 Pa s. This enabled both effectively inviscid and viscous jets to be investigated. To determine the effect of altering surface tension, *n*-butanol was added to two solutions (water and an 80% by volume glycerol solution) to lower the surface tension to below that of water. This extended the range of surface tension investigated to 65–100% that of water (0.047–0.072 $N\,m^{-1}$). The rotational speed of the can was varied from 50 to 300 rpm ($\Omega = 5.24$–$31.4\ rad\,s^{-1}$). The full experimental conditions used are given in Table 1.

## 3. Results and discussion

### 3.1. Break-up mechanism and prediction of break-up regime

Over the range of experimental parameters studied, four different break-up modes (defined in this paper as M1, M2, M3 and M4) were identified. For each mode, considerable differences in the mechanism of break-up and in the drop size distributions produced were observed. Each mode of break-up is described in detail below.

*Mode 1 (M1, Fig. 2)*. Rapid formation of primary droplets close to the orifice, with few or absence of satellite droplets. Varicose surface tension driven disturbances on the jet surface are convected downstream until they are sufficiently large that the primary drops form by capillary pinch-off. According to Ohnesorge (1936) and Chigier and Reitz (1995), M1 break-up can be expected from a straight jet with $Re < 400$, $We < 5$ and low jet exit velocities. Some similarity was observed here when the jet trajectories were least curved; in this work this occurs for a water jet emanating from a 0.001-m orifice at low rotation rates. The formation of occasional random satellite droplets may be caused by external disturbances acting on the jet, i.e., shaking of the can due to transmission of mechanical vibrations from the drive motor and gearbox.

*Mode 2 (M2, Fig. 3)*. Rapidly growing varicose disturbances of short wavelength are visible on the surface. The formation of the primary droplets is due to capillary pinch off, however, here satellite drops are formed in-between the primary droplets from fragments of fluid created by the break off of the primary drop. The jet break-up mode changed from M1 to M2 when the jet exit velocity was increased, either by increasing orifice size from 0.001 to 0.0003 m or increasing rotation rate ($100 < Re < 1500$, $5 < We < 25$).

*Mode 3 (M3, Fig. 4)*. Varicose long wavelength (2–5 times the jet diameter) disturbances are visible on the jet surface, with the jet breaking up simultaneously at several points along the curved jet into a continuous stream of droplets. Satellite droplets are again formed from the

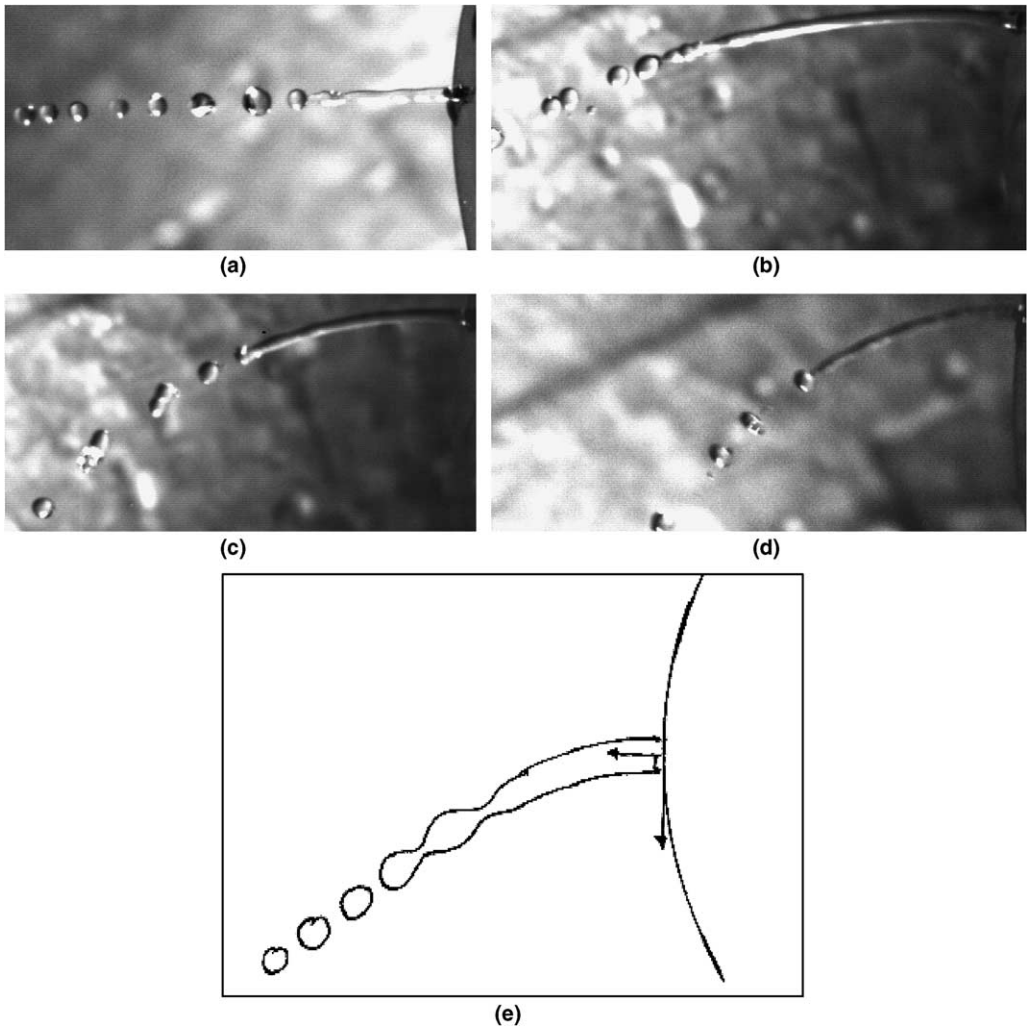


Fig. 2. Features of Mode 1 break-up with increasing rotational speed with a 0.001-m orifice: (a) $Rb = \infty$ (0 rpm), $U = 0.764\ \mathrm{m\,s^{-1}}$; (b) $Rb = 3.53$ (50 rpm), $U = 0.785\ \mathrm{m\,s^{-1}}$; (c) $Rb = 1.81$ (100 rpm), $U = 0.806\ \mathrm{m\,s^{-1}}$; (d) $Rb = 1.00$ (200 rpm), $U = 0.891\ \mathrm{m\,s^{-1}}$. $Oh = 0.005$ ($\eta = 0.0001$ Pa s; $\rho = 998.1\ \mathrm{kg\,m^{-3}}$); (e) sketch of Mode 1 break-up.

contraction of liquid threads connecting the primary droplets. This mode occurs when jets are created with high exit velocities using fluids with high dynamic viscosities. Since high viscosity dampens out the surface instabilities it is expected that a viscous jet would be more stable than an inviscid jet (Wallwork, 2002). Only long wavelength disturbances are observed at this condition.

*Mode 4 (M4, Fig. 5)*. Strongly non-linear disintegration is observed: the jet first elongates and emaciates and a swell develops at its end. The inertia of the swell causes the end of the jet to bend away from the can which alters the trajectory of the attached jet. The jet eventually becomes so tenuous that it shatters to form satellite droplets and the remaining jet recoils. This mode occurs for highly viscous jets at low exit velocities. Here the jet elongates because of the reduced instability caused by high viscosity, and the tip of the jet is observed to bend in the opposite direction

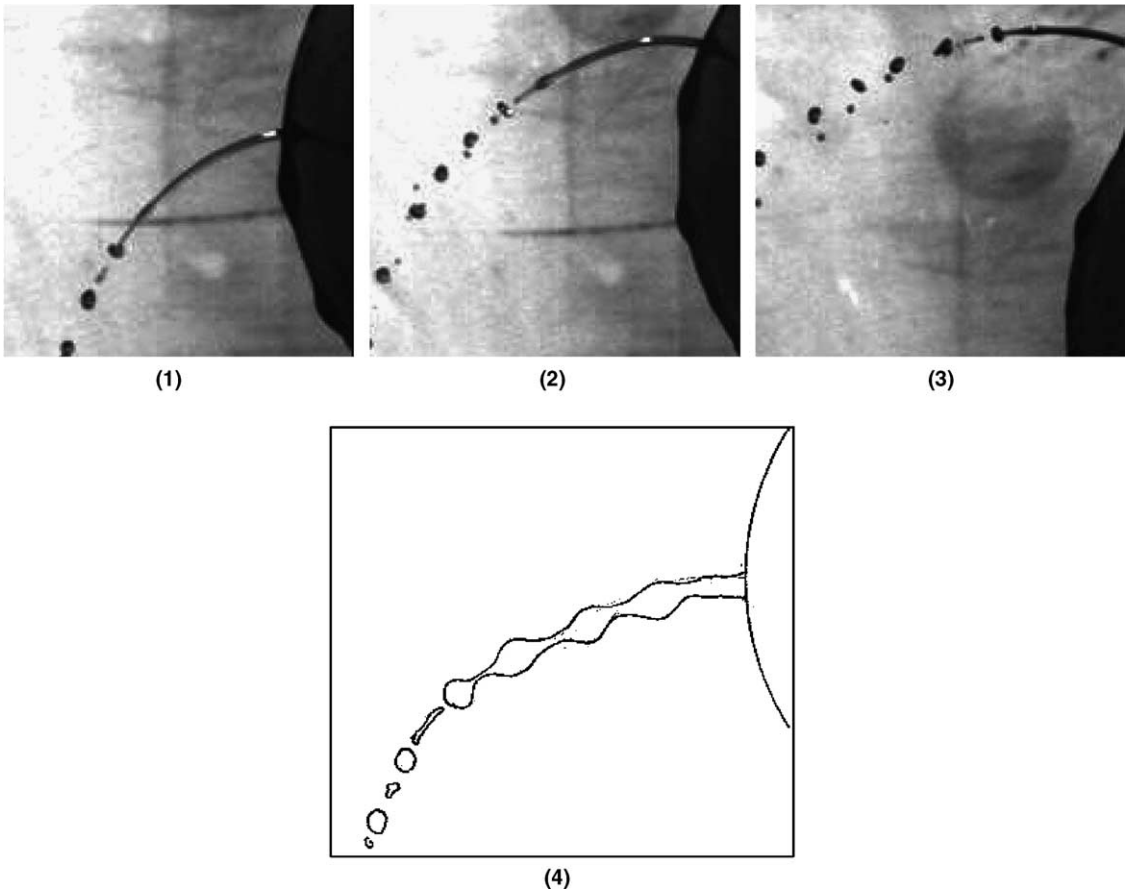


Fig. 3. Sequence (1–3) of Mode 2 break-up with a 0.001-m orifice at $Rb = 1.06$ (200 rpm): $U = 0.944$ m s$^{-1}$; $Oh = 0.0095$ ($\eta = 0.00181$ Pa s; $\rho = 1054.2$ kg m$^{-3}$); (4) sketch of Mode 2 break-up.

as shown in Fig. 5, sequences 1–4. Hence disturbances are convected upstream, which is unique feature of this mode.

The modes of break up depend upon the different influences of liquid inertia, liquid viscosity, surface tension and rotation rate acting on the jet. Using dimensional analysis a number of dimensionless groups were identified (Table 1) which allows the influence of the various parameters to be elucidated.

The break-up mode observed is a strong function of liquid dynamic viscosity and jet exit velocity. A plot of *Oh* against *We* as shown in Fig. 6a clearly groups together the data for each mode and hence break-up mode can clearly be predicted from this plot over the range of operating parameters studied.

Introduction of the rotation rate into the prediction complicates the analysis; since the jet exit velocity is affected by the centrifugal forces generated due to the rotation of the can, these two variables are coupled. A plot of *Oh* against *Rb* (Fig. 6b) illustrates that regions corresponding to M1/M2, M2/M3 and M4 can be identified. To identify the influence of rotation upon break-up

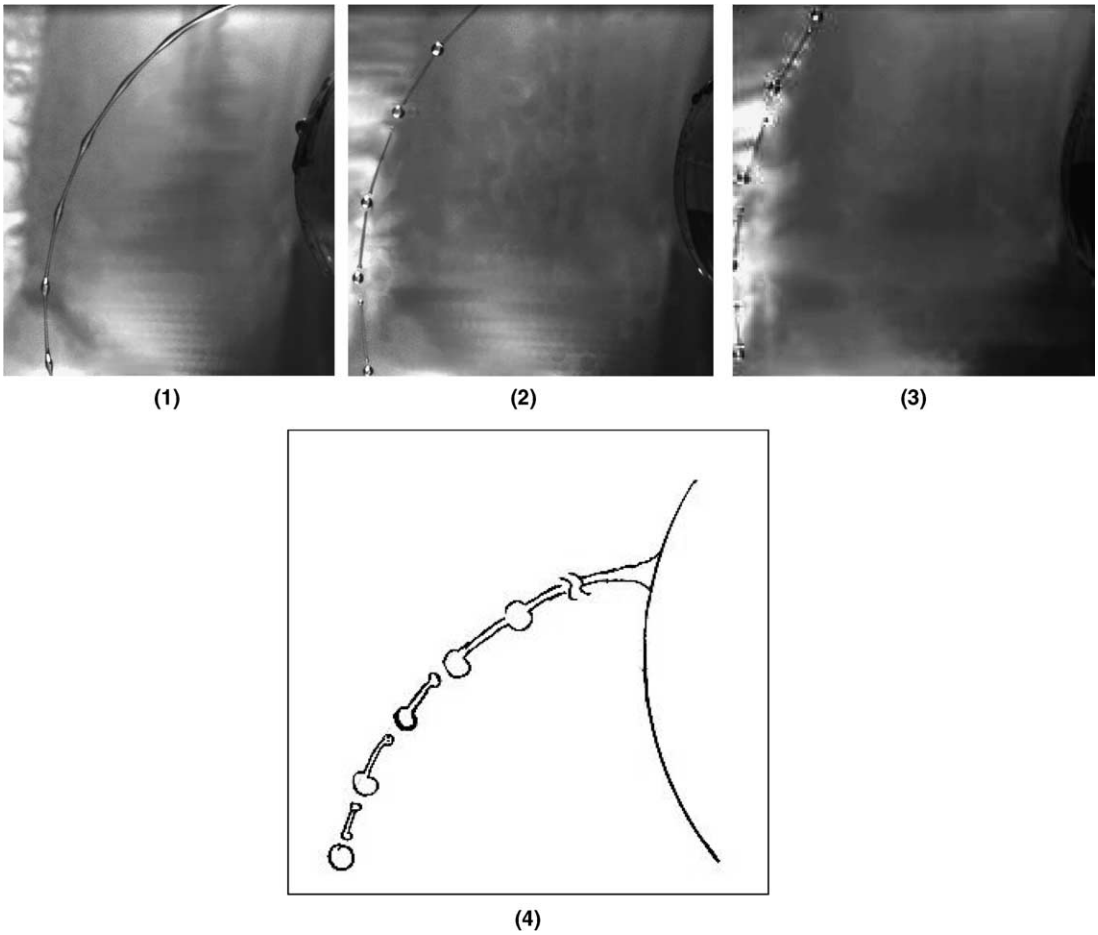


Fig. 4. Sequence (1–3) of Mode 3 break-up with a 0.003-m orifice which resembles a Rayleigh type mode: $Rb = 0.80$ (200 rpm); $U = 0.642\ \mathrm{m\,s^{-1}}$; $Oh = 0.241$ ($\eta = 0.0817$ Pa s; $\rho = 1215.5\ \mathrm{kg\,m^{-3}}$); (4) sketch of Mode 3 break-up.

alone without considering exit velocity, a plot of $Oh$ versus $Fr/Rb$ is shown in Fig. 6c. Here, we define $Fr$ as

$$Fr = \frac{U}{\sqrt{gH}}, \tag{1}$$

where $H$ is the height of liquid in the can above the nozzle (hydrostatic head). Hence this dimensionless number is a ratio of the exit velocity to the velocity which would be expected due to hydrostatic head in the can (ignoring losses due to the orifice). Hence

$$Fr/Rb = \frac{\Omega s_o}{\sqrt{gH}}, \tag{2}$$

which is independent of exit velocity. Fig. 6c shows that the data cannot be grouped using this parameter, although at low $Oh$, M1 is seen to occur predominantly at values of $Fr/Rb < 1$, while

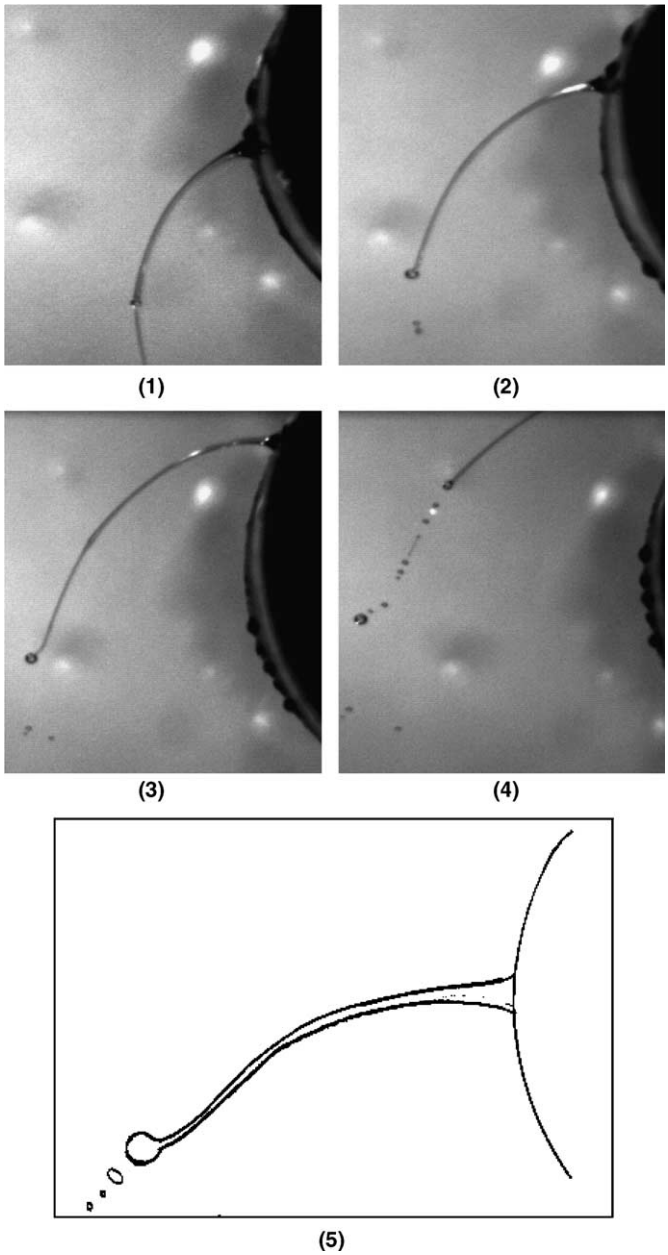


Fig. 5. Sequence (1–4) showing dynamics of Mode 4 break-up and recoiling phenomenon with a 0.001-m orifice: $Rb = 0.32$ (250 rpm); $U = 0.352\ \mathrm{m\,s^{-1}}$; $Oh = 0.233$ ($\eta = 0.0451$ Pa s; $\rho = 1202.6\ \mathrm{kg\,m^{-3}}$); (5) sketch of Mode 4 break-up.

M2 occurs mainly at $Fr/Rb > 1$. At high $Oh$, M3 and M4 occur over the whole range of $Fr/Rb$. This is an important result since it shows that break-up mode cannot be predicted from rotation rate and fluid properties alone; knowledge of the jet exit velocity is essential. This is inconvenient in the industrial context since whilst fluid properties and rotation rate are easily measured,

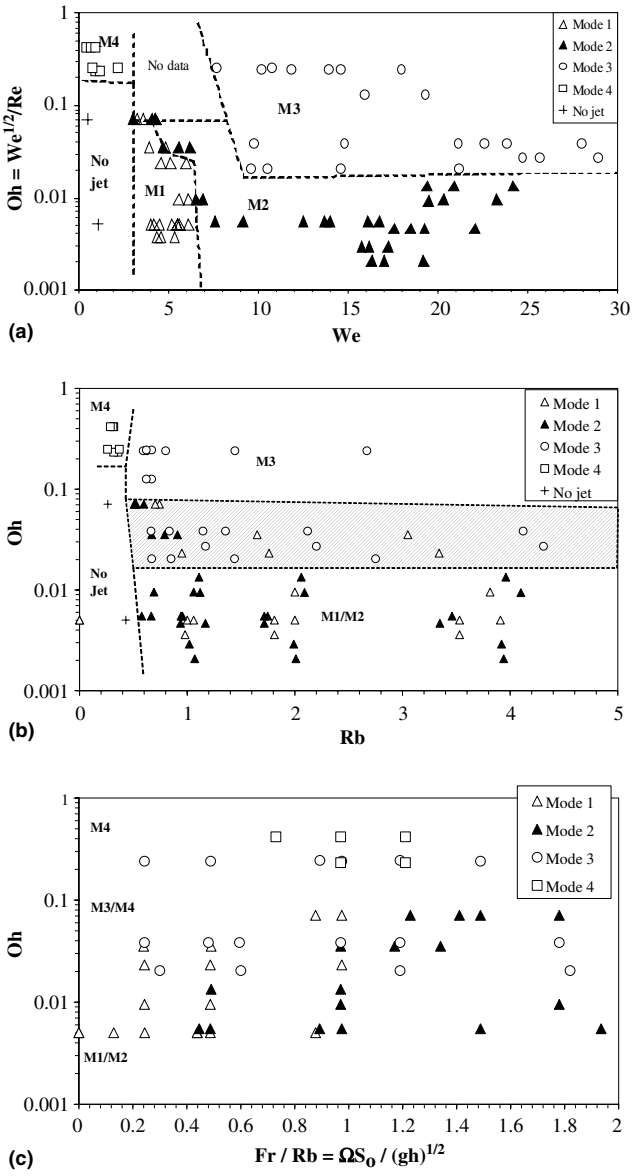


Fig. 6. Break-up regime maps: (a) *Oh* versus *We*, (b) *Oh* versus *Rb* and (c) *Oh* versus *Fr*/*Rb*.

measurement of jet exit velocity is more complex. The influence of rotation rate on jet exit velocity is discussed later.

Under the flow conditions for M4 break-up, the jet had difficulty in emanating from the can orifice which brings into question the "absolute stability" of the jet as described by Lin and Reitz (1998). If conditions for absolute stability are not met a coherent jet is not formed at the orifice and the jet breaks-up or drips almost immediately as it leaves the orifice. Reducing the rotation

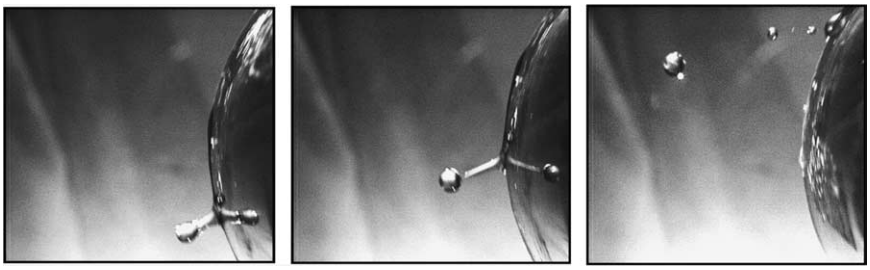

Fig. 7. Absence of coherent jet when $We \leqslant 1$: $Rb = 0.43$ (200 rpm); $U = 0.384\ \mathrm{m\,s^{-1}}$; $Oh = 0.005$ ($\eta = 0.001$ Pa s; $\rho = 998.1\ \mathrm{kg\,m^{-3}}$); $\sigma = 0.0724\ \mathrm{N\,m^{-1}}$.

rate (and hence the jet exit velocity) further, it was possible to observe this phenomenon at values of $We < 1$ as shown in Fig. 7. This perhaps corresponds with the occurrence of a singularity at $We = 1$ in the steady non-linear model of Wallwork (2002). This singularity was also found in the work of Baird and Davidson (1962), Finnicum et al. (1993) and Ramos (1996).

*3.1.1. Effect of rotation upon exit velocity and break-up length*

As mentioned previously, centrifugal forces generated by the spinning can affect the exit velocity of the jet as it emanates from the orifice. By performing a steady-state energy balance on the fluid, it can be easily shown that the velocity of the jet exiting from the orifice when the can is stationary can be described by

$$U_o = C_D\sqrt{2gH}, \tag{3}$$

where $U_o$ is the exit velocity at $\Omega = 0$ and $C_D$ is a drag coefficient incorporating losses due to friction in the fluid and nozzle and internal flows patterns and movement of the free surface inside the can. For the current experimental configuration, $C_D$ was calculated from the values of $U_o$ as ranging between 0.55 and 0.65 depending on fluid dynamic viscosity. These values are typical for orifices of this type. As $\Omega$ increases above zero, a centrifugal acceleration component, $s_o\Omega^2$ augments the gravitational force and the exit velocity hence increases. This effect is illustrated in Fig. 8 and shows that the exit velocity increases to 150% of the static value at the highest rotation rates used in this study. The increase is quadratic in $\Omega$ (as expected) and a weak function of $Oh$ (and hence viscosity). For the data shown, a general slow transition between M1 and M2 break-up is observed over a range of $Fr/Rb$ centred at $Fr/Rb \approx 1$. This is attributed to the increase in jet velocity at higher rotation rates.

The stability diagram for a straight jet is usually presented as a plot of break-up length versus jet exit velocity which allows the various regimes to be elucidated. However, a plot of this type for the spiralling case (i.e., break-up length versus either $Re$ or $We$) produces no conclusive trend. For different viscosity fluids, break-up length can either increase or decrease over the same range of $Re$ or $We$ as shown in Table 2. If a plot of dimensionless break-up length versus $Fr/Rb$ is considered, a general trend does emerge. Since only break-up lengths for M1 and M2 can be measured with confidence (Table 2), only these are plotted in Fig. 9. The data seem to indicate that break-up length passes through a minimum at $Fr/Rb \approx 1$ and eventually reaches a plateau at $Fr/Rb \approx 1.7$–2. Jet break-up is due to capillary pinch off over this entire range of $Fr/Rb$ (Figs. 2 and 3). This

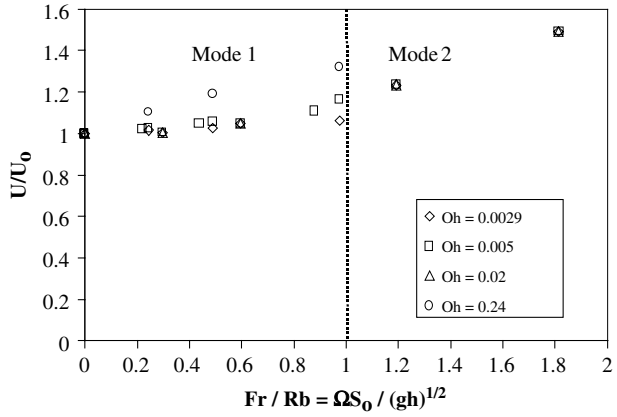


Fig. 8. Influence of rotation rate upon exit velocity of jet for different viscosity fluids ($0.0029 < Oh < 0.24$).

Table 2
Table of normalised break-up lengths for experiments using 0.001-m orifice and predictions from the linear instability model

| Visc. $\times 10^{-3}$ (Pa s) | $N$ | $We$ | $Rb$ | $Re$ | Inviscid break-up length divided by initial jet radius | | |
|---|---|---|---|---|---|---|---|
| | | | | | Experimental value (±SD) | Model prediction | Break-up mode |
| 1 | 50 | 4.3 | 3.5 | 410.3 | 50.2 ± 4.8 | 45.0 | M1 |
| 1 | 100 | 4.5 | 1.8 | 421.4 | 45.6 ± 4.2 | 47.6 | M1 |
| 1 | 200 | 5.5 | 1.0 | 465.8 | 43.8 ± 6.2 | 55.2 | M1 |
| 1.8 | 50 | 5.5 | 3.8 | 247.2 | 52.6 ± 2.9 | 50.2 | M1 |
| 1.8 | 100 | 6.1 | 2.0 | 259.6 | 50.2 ± 5.0 | 53.6 | M1 |
| 1.8 | 200 | 6.9 | 1.1 | 275.0 | 62.8 ± 7.0 | 61.2 | M2 |
| 4.5 | 50 | 4.9 | 3.3 | 92.3 | 51.8 ± 2.6 | 46.8 | M1 |
| 4.5 | 100 | 5.1 | 1.8 | 97.5 | 49.6 ± 3.3 | 50.2 | M1 |
| 4.5 | 200 | 6.0 | 1.0 | 105.0 | 58.0 ± 6.0 | 65.2 | M2 |
| 6.9 | 50 | 3.9 | 3.1 | 56.1 | 35.0 ± 3.3 | 44.2 | M1 |
| 6.9 | 100 | 4.9 | 1.7 | 62.3 | 44.6 ± 3.8 | 49.2 | M1 |
| 6.9 | 200 | 5.6 | 0.9 | 66.7 | 62.2 ± 6.8 | 57.0 | M2 |
| 6.9 | 250 | 6.2 | 0.8 | 70.2 | 72.2 ± 7.8 | 64.6 | M2 |
| 13.6 | 180 | 3.3 | 0.7 | 25.4 | 45.2 ± 3.6 | 45.8 | M1 |
| 13.6 | 200 | 3.6 | 0.7 | 26.8 | 52.8 ± 3.6 | 48.4 | M1 |
| 13.6 | 250 | 4.1 | 0.6 | 28.4 | 57.6 ± 6.8 | 53.6 | M2 |
| 13.6 | 290 | 4.3 | 0.53 | 29.1 | 81.6 ± 5.9 | 56.0 | M2 |

result is important since it appears that the increase of exit velocity due to centrifugal forces has a noticeable effect on the break-up length of the jet, despite having a weaker influence on the actual mode of break-up. Additionally, increasing the rotation rate results in a more curved jet trajectory as described by Wallwork et al. (2002).

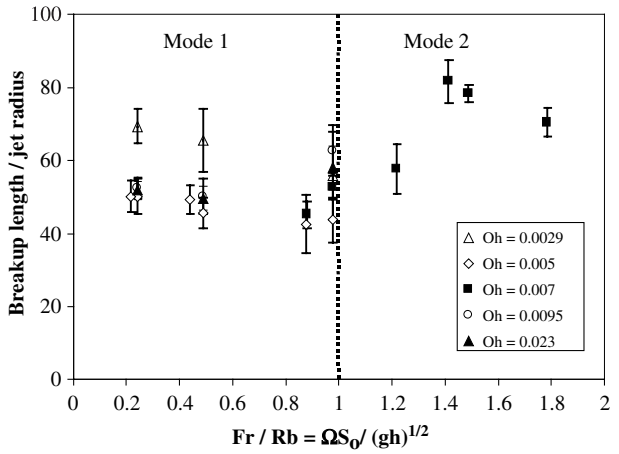


Fig. 9. Influence of rotation rate and exit velocity upon break-up length of the spiralling jet in Modes 1 and 2 for different viscosity fluids ($0.0029 < Oh < 0.023$).

### 3.1.2. Effect of operating parameters upon jet exit angle

Fig. 10 shows that upon decreasing the Rossby number (i.e., increasing the rotation rate) the jet exit angle, $\alpha$ (i.e., the angle between the centre line of the jet and the tangent at the orifice) is no longer orthogonal. This was taken as an assumption in the theoretical work by Wallwork et al. (2002) and Decent et al. (2002), together with the assumption of solid body rotation of fluid in the rotating can. A series of controlled experiments carried out using particle image velocimetry (PIV) showed that the assumption of solid-body rotation of fluid in the can was valid. A likely explanation for the changing jet exit angle is deviation caused by the creation of a thin viscous boundary layer at the can surface created from the action of the air close to the spinning can. This boundary layer only influences the jet very close to the can surface since the Reynolds number of the air is of the order of several thousand and the diffusion of vorticity from this boundary layer is very slow. The observed jet trajectories and break-up modes are not dependent upon a long timescale, as might be expected if the airflow was important because this diffusion of vorticity

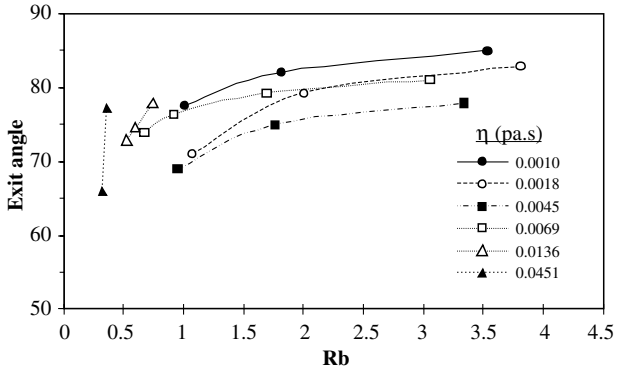


Fig. 10. Exit angle in relation to Rossby number for water–glycerol solutions.

would gradually envelope the jet. Also, the paper of Wallwork et al. (2002) found excellent agreement between theoretical and experimental descriptions for the jet trajectory over the same parameter ranges as used here. This evidence indicates that the air flow is unimportant in these experiments but is likely to have more influence on the industrial scale where the ranges of rotation rate and *Re* of both fluid and air are much larger.

### 3.1.3. Theoretical prediction of break-up length

The theoretical break-up lengths estimated from the linear stability analysis are given in Table 2. Full details of this analysis are given in Wallwork et al. (2002) which for the sake of brevity is summarised here. The equation for the non-dimensionalised break-up length $s^*$ is

$$\left| \frac{AI_1(k^*(s^*)R_0(s^*))}{\mathrm{i}(k^*(s^*)u_0(s^*) - \omega(s^*))} \exp(\mathrm{i}k^*(s^*)s^*/\varepsilon) \right| = R_0(s^*), \tag{4}$$

where the break-up occurs at $s = s^*$ and $s$ is the non-dimensionalised arclength along the jet. Here $R$ is the non-dimensionalised radius of the jet, $\varepsilon$ is the ratio of the orifice to the radius of the can and $u_0$ is the non-dimensionalised jet velocity at its centreline. The equations for $u_0(s)$ and $R_0(s)$ are given by the following differential equations and initial conditions:

$$u_0 = \left(1 + \frac{X^2 + 2X + Z^2}{Rb^2} + \frac{2}{We}\left(1 - \frac{1}{R_0}\right)\right)^{1/2}, \tag{5}$$

$$\frac{\mathrm{d}R_0}{\mathrm{d}s} = -\frac{WeR_0^2((X+1)X_s + ZZ_s)}{Rb^2(2WeR_0u_0^2 + 1)}, \tag{6}$$

$$\frac{\mathrm{d}^2Z}{\mathrm{d}s^2} = \frac{WeR_0X_s}{WeR_0u_0^2 - 1}\left(\frac{2u_0}{Rb} + \frac{ZX_s - (X+1)Z_s}{Rb^2}\right), \tag{7}$$

$$X_s^2 + Z_s^2 = 1, \tag{8}$$

$$u_0(s=0) = R_0(s=0) = X_s(s=0) = 1 \tag{9}$$

and

$$X(s=0) = Z(s=0) = Z_s(s=0) = 0. \tag{10}$$

$X$ and $Z$ are orthogonal co-ordinates which describe the centre-line of the jet trajectory [$X(s,t) + s_0$, 0, $Z(s,t)$ in the Cartesian co-ordinate system]. The wavenumber $k(s)$ and the frequency $\omega(s)$ are related by the eigenvalue relationship:

$$\mathrm{i}(\omega - ku_0) \pm \sqrt{\frac{1}{We}\left(\frac{1}{R_0^2} - k^2\right)k\frac{I_1(kR_0)}{I_0(kR_0)}} = 0, \tag{11}$$

where $I_i$ are modified Bessel functions of order $i$. Given a streamwise velocity component at the orifice at $s = 0$

$$U(1 + 2\mathrm{Re}(A)\cos(\omega t) - 2\mathrm{Im}(A)\sin(\omega t)) \tag{12}$$

so that $A$ measures the amplitude of the wave-like velocity perturbation to the steady state and $t$ is time, the above non-linear algebraic eigenvalue relationship (12) may be solved to find the

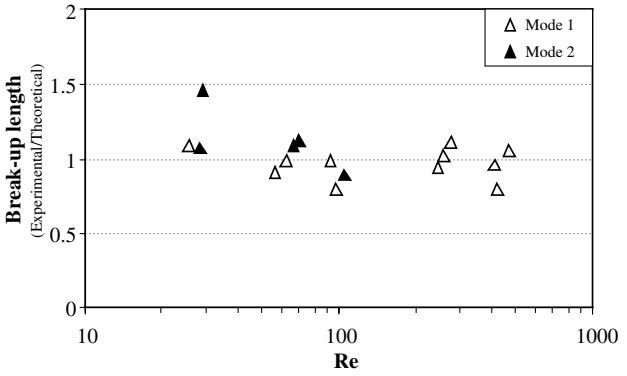


Fig. 11. Comparison of experimental and theoretical break-up lengths for various Reynolds numbers.

(complex) wavenumber $k$ as a function of the arclength $s$ along the jet. Then $k^*(s)$ is the most unstable of all the possible solutions for $k(s)$ i.e., the one with the most negative imaginary part. By solving the break-up equation for $s^*$, the dimensional break-up is then equal to $s_0 s^*$.

The general trend predicted by this theory in Wallwork et al. (2002) was for the dimensionless break-up length to increase with either *We* or *Re*. Fig. 11 shows better agreement between the experimental and theoretical prediction of break-up length for small Reynolds numbers, i.e., in the case of more viscous jets but this is not the case for less viscous jets which are at conditions closer to those assumed in the analysis. The experimental observations described in this paper indicate that modelling of these phenomena therefore requires a full non-linear analysis. Recent work by Parau et al. (2003) details a non-linear spatial instability analysis of the process by the numerical computation of the one-dimensional equations. They arrive at a model which can predict the evolution of disturbances on the jet surface and hence the size of the main and satellite droplets can be derived.

The reduction in surface tension of the fluid caused by the addition of *n*-butanol to the fluid causes the break-up length of the jet to reduce in the case of less viscous jets. Nonetheless the break-up mode was not dissimilar from the reference case, i.e., pure distilled water. The opposite effect was observed for the most viscous fluids used. The jets became more elongated and tenuous which resulted in multiple break-up of the jet into different size droplets.

### *3.2. Mean drop size and size distributions*

To minimize the time required for the analysis of one population of drop sizes, it is desirable to measure as few droplets as possible. However, the number must be sufficient to give a representative sample, which is dependent upon the width of the drop size distribution and this must be assessed. Wu et al. (1995) reported using 40–200 droplets from experimental studies since their analysis was limited by the relatively small number of droplets formed. In another study by McCreery and Stoots (1996), each drop diameter distribution was based on as many as 10,000 individual drop measurements. In this study, preliminary drop size analysis was carried out by assessing 50, 100 and 200 droplets by means of image analysis software (Qwin 500, Leica). No significant variation was seen from the three sample sizes, as the difference in mean diameters

Table 3
Effect of sample size on mean drop diameter

| Mean diameter (mm) | Sample size | | |
|---|---|---|---|
| | 50 drops | 100 drops | 200 drops |
| $d_{10}$ | 0.996 | 0.985 | 0.956 |
| $d_{32}$ | 1.057 | 1.082 | 1.077 |
| $d_{43}$ | 1.069 | 1.097 | 1.094 |

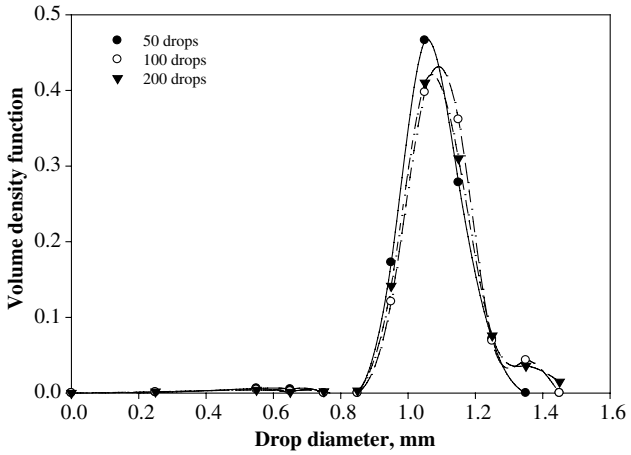


Fig. 12. Effect of the sample size on volume density function. For size classes based on a geometric series ratio of 1.142:0.001 m orifice: $Rb = 0.98$ (200 rpm); $Oh = 0.0036$ ($\eta = 0.001$ Pa s, $\rho = 998.1$ kg m$^{-3}$).

calculated from two consecutive samples was smaller than 5%, as shown in Table 3. Fig. 12 shows that the volume density distribution plots virtually overlap. It should be noted that to obtain the largest population, between 150 and 200 frames are required. Two image size settings were used i.e., $512\times480$ pixels and $256\times480$ pixels for respective frame rates of 500 and 250 frames per second. The accuracy of the measurements depended on the minimum drop size which could be measured by the software. This was between 5 and 7 pixels which translates as approximately $1\times10^{-4}$ m in absolute length. Only the first and immediate neighbouring droplets, particularly near the onset of break-up, were used. This is to minimize any optical effects as the jet in some cases falls significantly out of the horizontal plane containing the orifice due to gravitational forces. The size distribution plots shown here were obtained by assessing at least 200 individual droplets.

### *3.2.1. Effects of operating parameters and break-up mode on drop size distribution*

Examples of drop size distributions obtained for break-up modes M1–M4 are shown in Figs. 13–16, respectively. For M1 as shown in Fig. 13, the drop size distributions produced are unimodal, with the median drop size decreasing with increasing rotation rate. For M2 break-up, the drop size distributions are unsurprisingly bimodal, with the smallest peak indicating the size of the satellite droplets and the larger peak indicating the size of the main droplets (Fig. 14). Increasing

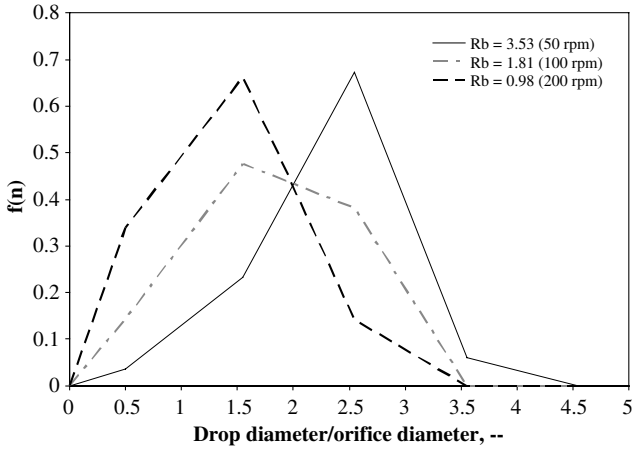


Fig. 13. Drop size distribution for three rotational rates: $Rb = 3.53, 1.81, 0.98$ (50, 100, 200 rpm) in break-up Mode 1 ($400 < Re < 500$; $We < 10$; $Oh = 0.005$ ($\eta = 0.001$ Pa s, $\rho = 998.1$ kg m$^{-3}$)).

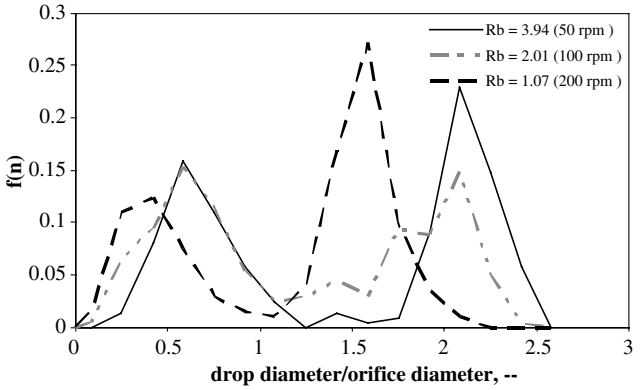


Fig. 14. Drop size distributions for three rotational rates: $Rb = 3.94, 2.01, 1.07$ (50, 100, 200 rpm) in break-up Mode 2 ($Re > 1,000$; $15 < We < 20$; $Oh = 0.0029$ ($\eta = 0.001$ Pa s, $\rho = 998.1$ kg m$^{-3}$)).

the rotation rate resulted in a shift of both main and satellite drop size distributions to smaller size ranges. For both modes M1 and M2, the primary drops are of sizes of the order of 1.5–3.5 times the jet diameter. Rayleigh (1878) stated that for straight jets, primary drop size would be of the order of a few times the jet diameter assuming that no satellite droplets were formed, as restated by Chigier and Reitz (1995).

The break-up mode M3 produced significant satellite droplets and the size was in the same order of magnitude as the orifice size from which the jet emerged, as shown in Fig. 15. Increasing the rotation rate again, resulted in an increase in number of satellite droplets formation at the expense of the main droplets. The sizes of the satellites droplets approach those of the main droplets.

As shown in Fig. 14, mode M2 break-up produces the largest ratio of primary droplets to orifice diameter than compared with other modes. This is due to the fact that in mode M2

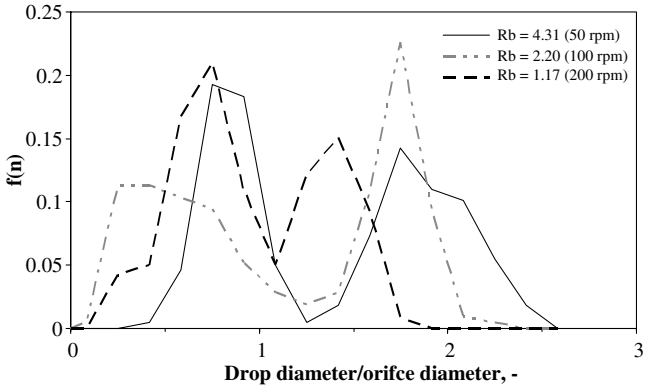


Fig. 15. Drop size distributions for three rotational rates: $Rb = 4.31, 2.20, 1.17$ (20, 100, 200 rpm) in break-up Mode 3 ($120 < Re < 150$; $20 < We < 30$; $Oh = 0.038$ ($\eta = 0.0129$ Pa s, $\rho = 1164.6$ kg m$^{-3}$)).

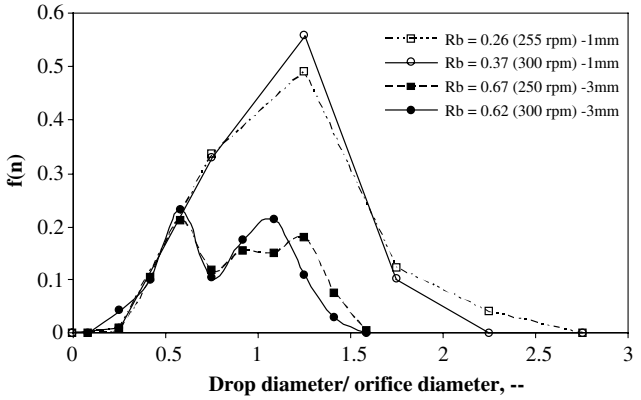


Fig. 16. Drop size distributions for two rotational rates: (a) $Rb = 0.67, 0.62$ (250, 300 rpm) in break-up Mode 3 with a 0.003-m orifice ($20 < Re < 25$; $15 < We < 20$; $Oh = 0.178$ ($\eta = 0.061$ Pa s, $\rho = 1215.5$ kg m$^{-3}$)); (b) $Rb = 0.26, 0.37$ (255, 300 rpm) in break-up Mode 4 with a 0.001-m orifice ($Re < 5$; $We < 3$; $Oh = 0.352$ ($\eta = 0.071$ Pa s, $\rho = 1215.5$ kg m$^{-3}$)).

break-up, the liquid thread between the primary droplets joins with one of the primary droplets when breaking off from the jet, instead of detaching to form another drop. In mode M3 break-up, these liquid threads detach from both primary droplets and shrink to from smaller satellite droplets. Hence in mode M3, the largest satellite droplets are produced. It is important to note that some drop collisions and merging of droplets were also observed, particularly in mechanisms where droplets are formed singly (modes M1 and M2). These collisions occasionally produced very large droplets up to approximately four times the diameter of the orifice. However, for modes where droplets were created by simultaneous multiple break-up (modes M3 and M4), this effect was not observed. Table 4 gives a summary of the drop sizes produced in each mode.

Fig. 16 shows that mode M4 break-up (represented by open round and square symbols) is dominated by the formation of satellite droplets as a result of the disintegration of the entire jet as it thins. A unimodal drop size distribution is produced. The effect of changing the orifice size from 0.001 to 0.003 m resulted in very different size distributions due to the change in break-up mode

Table 4
Drop sizes for each mode of break-up

| | Primary drop size (mm) | Satellite drop size (mm) | No. of satellite drops/10 primary drops formed |
|---|---|---|---|
| Mode 1 | $2.3 \leqslant d \leqslant 2.6$ | $0.72 \leqslant d \leqslant 0.85$ | 3–4 |
| Mode 2 | $4.7 \leqslant d \leqslant 6.3$ | $1.3 \leqslant d \leqslant 2.0$ | 6–12 |
| Mode 3 | $3.3 \leqslant d \leqslant 5.7$ | $1.7 \leqslant d \leqslant 2.5$ | 6–17 |
| Mode 4 | $1.6 \leqslant d \leqslant 1.9$ | $1.0 \leqslant d \leqslant 1.1$ | 51–88 |

from M4 to M3; M4 break-up gives a unimodal distribution whilst mode M3 break-up remains bimodal.

### 3.2.2. Effect of system parameters on drop sizes

The effect of viscosity on drop size can be seen in Fig. 17. With increasing Ohnesorge number (increasing viscosity), the size of the primary and satellite droplets decreases. Teng et al. (1995) also found that primary drop sizes were dependant on Ohnesorge number from a linear analysis. As viscosity increases, viscous forces act to damp out surface perturbations on the jet and retard wave growth. This allows the jet to remain intact for longer, increasing break-up length and eventually breaking up into droplets that are smaller in size.

Fig. 18 shows the effect of changing *Rb* on the drop size. In all break-up modes, increasing the rate of rotation (decreasing *Rb*) significantly reduces the main drop sizes (typically between 30% and 62%), although the satellite droplets were only marginally affected. The size distribution plots (Figs. 13–16) also confirm this. Narrower size distributions can also be expected at higher rotational rates.

An increase in the rotation rate always results in an increase of jet exit velocity and a more curved jet trajectory, which also causes a thinning of the jet as seen by Wong et al. (2003). Jets that are rotating at a high rotation rate produce smaller droplets. This rotation increased the growth rate to such an extent that it significantly reduced the length of break-up, which means that the

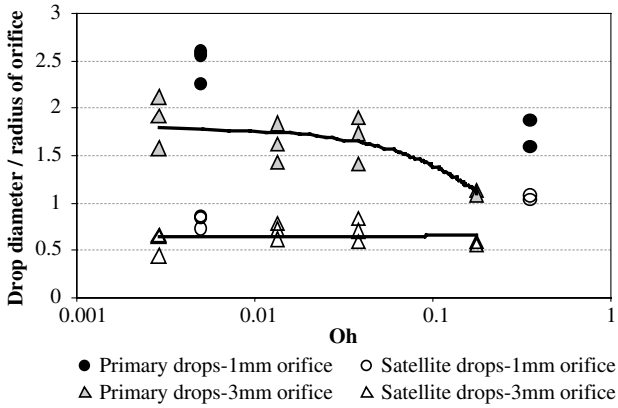


Fig. 17. Effect of Ohnesorge number on primary and corresponding satellite drop sizes.

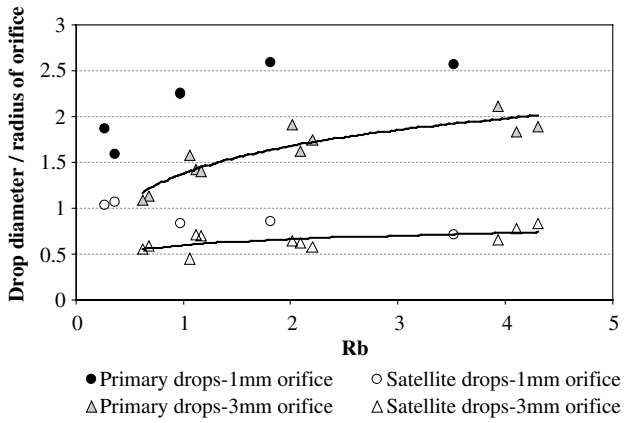


Fig. 18. Effect of Rossby number on primary and corresponding satellite drop sizes.

waves had less space to develop and thus a smaller wave amplitude at break-up produces a smaller drop.

Fig. 19 shows the effect of jet exit velocity on both primary and satellite drop sizes. There is no monotonic relationship between drop size and exit velocity from the results obtained in this work. The primary drop sizes generally increase as the exit velocity increases between 0.3 and 0.9 $m\,s^{-1}$. However, the trend then reverses for exit velocities between 0.9 and 1.05 $m\,s^{-1}$. The satellite droplets appear to reduce in size slightly. Based on the data available at present, a qualitative explanation is given here. For low exit velocities (small Reynolds numbers), the growth rate is determined by a balance of surface tension and viscous forces alone, while inertial forces are insignificant. As the exit velocity increases, the inertial forces become increasingly important and act to promote the growth rate of the disturbance. As the disturbance is convected by the mean flow, a further increase of jet exit velocity can result in the convection becoming fast enough to sweep disturbances away before they can grow, hence produce smaller droplets (Eggers, 1997).

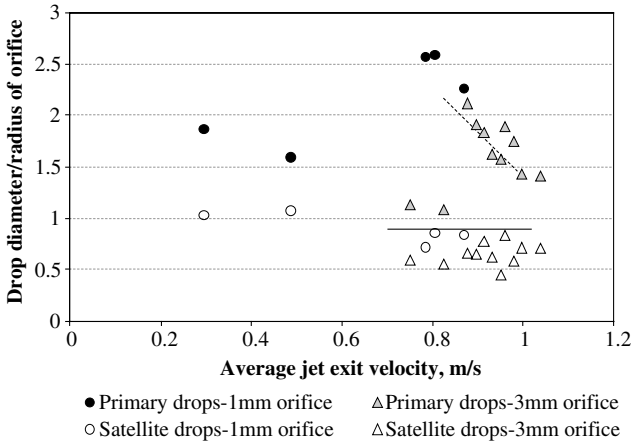


Fig. 19. Effect of average jet exit velocity on primary and corresponding satellite drop sizes.

## 4. Conclusions

A parametric study of the break-up and drop formation of curved liquid jets spun from a rotating can under ambient conditions was made. Over the range of experimental conditions, the mechanism of jet break-up falls in one of four different modes (M1–M4). Of all the parameters studied, liquid dynamic viscosity and jet exit velocity have the strongest influence on break-up mode which can be predicted from a plot of *Oh* versus *We*. The influence of rotation rate is more subtle since the influence on break-up mode is weak but there is a stronger influence on break-up length. Increasing the rotation rate (decreasing *Rb*) results in the trajectory of the jets becoming more curved and an increase in jet exit velocity due to centrifugal forces. At low *Oh* the break-up mode changes from M1 to M2 over a range of $Fr/Rb \approx 1$ which appears to correspond to an approximate minimum in the break-up lengths measured for M1/M2 break-up. This is related to an increase in jet exit velocity. At high *Oh*, M3 and M4 modes can exist for all the rotation rates studied.

Break-up lengths obtained from the experiments and from the linear model of Wallwork et al. (2002) and Decent et al. (2002) showed that break-up length of the jet is a complex function of the system parameters. The experimental data showed that use of the linear model is insufficient to predict break-up length in mode M1 and M2. A full non-linear theoretical analysis is needed.

Unimodal drop size distributions were obtained for M1 break-up and bimodal distributions were obtained for M2 break-up. Merging of droplets was observed in these two modes of break-up, and this resulted in the largest droplets being produced. The effect of increasing rotation rate showed a progressive decrease in the size of the larger (main) droplets whilst the size of the smaller (satellite) droplets were not significantly changed.

## Acknowledgements

The authors would like to acknowledge the financial support of the EPSRC (GR/R21349/01) and the contributions of Pankaj and Prakash Koria towards the drop size characterization work. Thanks are due to Lucy Partridge for some help with the jet exit velocity measurements.

## References

Baird, M.H.I., Davidson, J.F., 1962. Annular jets—I. Fluid dynamics. Chem. Eng. Sci. 17, 467–472.

Blaisot, J.B., Adeline, S., 2003. Instabilities on a free falling jet under an internal flow breakup mode regime. Int. J. Multiphase Flow 29, 629–653.

Bousfield, D.W., Denn, M.M., 1987. Jet break-up enhanced by an initial pulse. Chem. Eng. Comm. 53, 61–68.

Bousfield, D.W., Keunigs, G., Marrucci, G., Denn, M.M., 1986. Nonlinear-analysis of the surface-tension driven breakup of viscoelastic filaments. J. Non-Newton. Fluid Mech. 21, 79–97.

Camelot, D.M.A., Hartman, R.P.A., Marijnissen, J.C.M., Scarlett, B., Brunner, D., 1999. Experimental study of the jet break up for electrohydrodynamics atomisation of liquids in the cone-jet mode. J. Aerosol Sci. 30, 976–977.

Chaudhary, K.C., Redekopp, L., 1980. The nonlinear capillary instability of a liquid jet, Part I & II. J. Fluid Mech. 96, 263–286.

Chigier, N., Reitz, R.D., 1995. Regimes of jet breakup and breakup mechanisms—physical aspects. Prog. Astronaut. Aeronaut. 1, 109–135.

Decent, S.P., King, A.C., Wallwork, I.M., 2002. Free jets spun from a prilling tower. J. Eng. Math. 42, 265–282.
Donnelly, R.J., Glaberson, W., 1965. Experiments on the capillary instability of a liquid jet. Proc. R. Soc. Lond. 290, 547–556.
Eggers, J., 1997. Nonlinear dynamics and breakup of free-surface flows. Rev. Mod. Phys. 69, 865–929.
Finnicum, D.S., Weinstein, S.J., Ruschak, K.J., 1993. The effect of applied pressure on the shape of a two-dimensional liquid curtain falling under the influence of gravity. J. Fluid Mech. 255, 647–665.
Goedde, E.F., Yuen, M.C., 1970. Experiments on liquid jet instability. J. Fluid Mech. 40, 495–511.
Hilbing, J.H., Heister, S.D., 1996. Droplet size control in liquid jet break-up. Phys. Fluids 8, 1574–1581.
Keller, J.B., Rubinow, S.I., Tu, Y.O., 1973. Spatial instability of a jet. Phys. Fluids 16, 2052–2055.
Lin, S.P., Reitz, R.D., 1998. Drop and spray formation from a liquid jet. Ann. Rev. Fluid Mech. 30, 85–105.
Lindblad, N.R., Schneider, J.M., 1965. Production of uniform-sized droplets. J. Sci. Instrum. 42, 635–642.
McCreery, G.E., Stoots, C.M., 1996. Drop formation mechanism and size distributions for spray plate orifices. Int. J. Multiphase Flow 22, 431–452.
Meessen, J.H., Petersen, H., 1996. Urea. Ullmann's Encyc. Ind. Chem. A 27, 333–363.
Middleman, S., 1995. Modelling Axisymmetric Flows: Dynamics of Films, Jets and Drops. Academic Press, New York. pp. 94–123.
Moses, M.P., 1995. Visualization of liquid jet break-up and droplet formation. M.Sc. Thesis, Purdue University.
Ohnesorge, W., 1936. Formation of drops by nozzles and the breakup of liquid jets. Z. Angew. Math. Mech. 16, 355–358.
Parau, E., Decent, S.P., King, A.C., Simmons, M.J.H., Wong, D.C.Y., 2003. Nonlinear travelling waves on a spiralling liquid jet. J. Eng. Math., submitted.
Ramos, J.I., 1996. Upward and downward annular liquid jets: conservation properties, singularities, and numerical errors. Appl. Math. Model. 20, 44–458.
Rayleigh, L., 1878. On the stability of jets. Proc. Lond. Math. Soc. 10, 4–13.
Rutland, D.F., Jameson, G.J., 1971. A non-linear effect in the capillary instability of liquid jets. J. Fluid Mech. 46, 267–275.
Savart, F., 1833. Memoire sur la Constitution des Veines Liquides lancees par des orifices circulaires en mince paroi. Ann. Chim. Phys. 53, 337–386.
Shield, T.W., Bogy, D.B., Denn, M.M., 1987. Drop formation by DOD ink-jet orifices: a comparison of experimental and numerical simulation. IBM J. Res. Dev. 31, 96–110.
Taub, H.H., 1976. Investigation of nonlinear waves on liquid jets. Phys. Fluids 46, 1124–1129.
Teng, H., Kinoshita, C.M., Masutani, S.M., 1995. Prediction of droplet size from the breakup of cylindrical liquid jets. Int. J. Multiphase Flow 21, 129–136.
Torpey, P.A., 1989. A nonlinear theory for describing the propagation of disturbances on a capillary jet. Phys. Fluids 1, 66–71.
Wallwork, I.M., 2002. The trajectory and stability of a spiralling liquid jet. Ph.D. Thesis, The University of Birmingham, UK.
Wallwork, I.M., Decent, S.P., King, A.C., Schulkes, R.M.S.M., 2002. The trajectory and stability of a spiralling liquid jet: Part 1. Inviscid theory. J. Fluid Mech. 459, 43–65.
Weber, C., 1931. Zum zerfall eines flussigkeitsstrahles. Z. Angew. Math. Mech. 11, 136–141.
Wong, D.C.Y, Simmons, M.J.H., King, A.C., Decent, S.P., Parau, E., 2003. Dynamic break-up and drop formation from a liquid jet spun from a rotating orifice. Part 1: Experimental. In: Proc. FEDSM'03, IBSN 0-7918-3673-8, FEDSM2003-45148.
Wu, P.K., Miranda, R.F., Faeth, G.M., 1995. Effects of initial flow conditions on primary break-up of non turbulent and turbulent round liquid jets. Atom. Sprays 5, 175–196.